iScience

CellPress
OPEN ACCESS

Article

The wall-less bacterium *Spiroplasma poulsonii* builds a polymeric cytoskeleton composed of interacting MreB isoforms

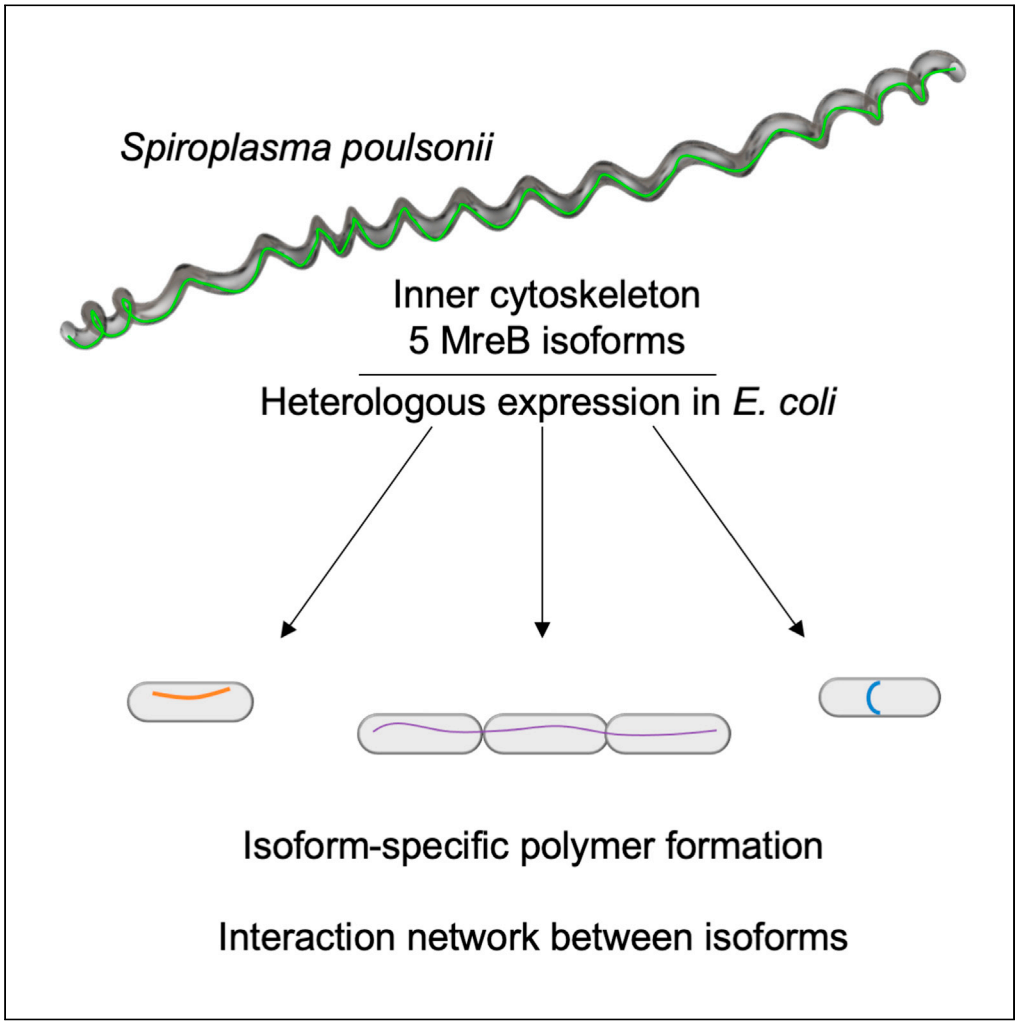

Florent Masson,
Xavier Pierrat,
Bruno Lemaitre,
Alexandre Persat

florent.masson@epfl.ch (F.M.)
alexandre.persat@epfl.ch (A.P.)

Highlights

The five *Spiroplasma* MreB isoforms are extremely abundant proteins *in vivo*

Each isoform produces filaments when expressed in a heterologous system

SpMreBs form an interaction network that regulates filament length and shape

Masson et al., iScience *24*, 103458
December 17, 2021
https://doi.org/10.1016/j.isci.2021.103458

iScience

CellPress
OPEN ACCESS

Article

The wall-less bacterium *Spiroplasma poulsonii* builds a polymeric cytoskeleton composed of interacting MreB isoforms

Florent Masson,[1,*] Xavier Pierrat,[1,2] Bruno Lemaitre,[1] and Alexandre Persat[1,2,3,*]

SUMMARY

A rigid cell wall defines the morphology of most bacteria. MreB, a bacterial homologue of actin, plays a major role in coordinating cell wall biogenesis and defining cell shape. *Spiroplasma* are wall-less bacteria that robustly grow with a characteristic helical shape. Paradoxal to their lack of cell wall, the *Spiroplasma* genome contains five homologs of MreB (SpMreBs). Here, we investigate the function of SpMreBs in forming a polymeric cytoskeleton. We found that, *in vivo*, *Spiroplasma* maintain a high concentration of all MreB isoforms. By leveraging a heterologous expression system that bypasses the poor genetic tractability of *Spiroplasma*, we found that SpMreBs produced polymeric filaments of various morphologies. We characterized an interaction network between isoforms that regulate filament formation and patterning. Therefore, our results support the hypothesis where combined SpMreB isoforms would form an inner polymeric cytoskeleton *in vivo* that shapes the cell in a wall-independent manner.

INTRODUCTION

Bacteria grow into an astonishing variety of shapes including spheres, straight and curved rods, disks, trapezoids, helices, and even stars (Kysela et al., 2016). The stability of these morphologies within each species suggests that they confer important fitness advantages in the natural ecological niches of these microbes (Young, 2006). Bacteria typically maintain their morphologies by virtue of their rigid cell wall (Cabeen and Jacobs-Wagner, 2005). Local constraining of cell wall peptidoglycan patterning by short MreB polymers provides a cell with its shapes (Wagstaff and Löwe, 2018). As a consequence, degrading the bacterial cell wall is sufficient to relax its shape into a spherical membrane (Billings et al., 2014; Wu and Errington, 1998). In contrast, most mammalian cells are plastic and actively control their shapes by virtue of a dynamic actin cytoskeleton (Svitkina, 2018).

All but one bacterial family (Mollicutes) synthesize a peptidoglycan cell wall. The cell envelope of Mollicutes is essentially a lipid bilayer. Mollicutes underwent a genome reduction, including loss of cell wall synthesis genes, by regressive evolution upon their adaptation to a strict host-associated lifestyle (Bové, 1993; Trachtenberg, 1998). As one could expect from their lack of cell wall, the class encompasses genera such as *Mycoplasma* and *Phytoplasma* with no distinctive cell shape, adapting their morphology to the constraints of their close environment (Ku et al., 2014). *Spiroplasma* makes exception as this genus is uniformly composed of long, helical bacterial species (Gasparich, 2002) (Figure 1A and Video S1). Furthermore, *Spiroplasma* cells actively deform their body to propel themselves in high-viscosity fluid environments (Shaevitz et al., 2005; Trachtenberg and Gilad, 2001). How does *Spiroplasma* maintain and actively controls its morphology? No external rigid structure has been identified in these bacteria. We therefore hypothesize that, by analogy with eukaryotes, an internal cytoskeleton maintains *Spiroplasma* membrane morphology.

Early electron cryotomograms of *Spiroplasma* have revealed intracellular filament that may function as a membrane-associated cytoskeleton (Kürner et al., 2005). One candidate protein called fibril (Fib), whose polymerization forms an internal ribbon spanning the entire length of the bacterium, may provide structural support for the membrane (Kürner et al., 2005; Sasajima et al., 2021; Townsend and Plaskitt, 1989; Trachtenberg et al., 2008; Trachtenberg and Gilad, 2001; Williamson, 1974). Therefore, Fib was initially thought to be necessary and sufficient to maintain the helical shape of *Spiroplasma*. Yet, the serendipitous isolation of non-helical *Spiroplasma* variant still harboring fibrils indicates that Fib is not sufficient to maintain helical

[1]Global Health Institute, School of Life Sciences, École Polytechnique Fédérale de Lausanne (EPFL), 1015 Lausanne, Switzerland

[2]Institute of Bioengineering, School of Life Sciences, École Polytechnique Fédérale de Lausanne (EPFL), 1015 Lausanne, Switzerland

[3]Lead contact

*Correspondence: florent.masson@epfl.ch (F.M.), alexandre.persat@epfl.ch (A.P.)

https://doi.org/10.1016/j.isci.2021.103458

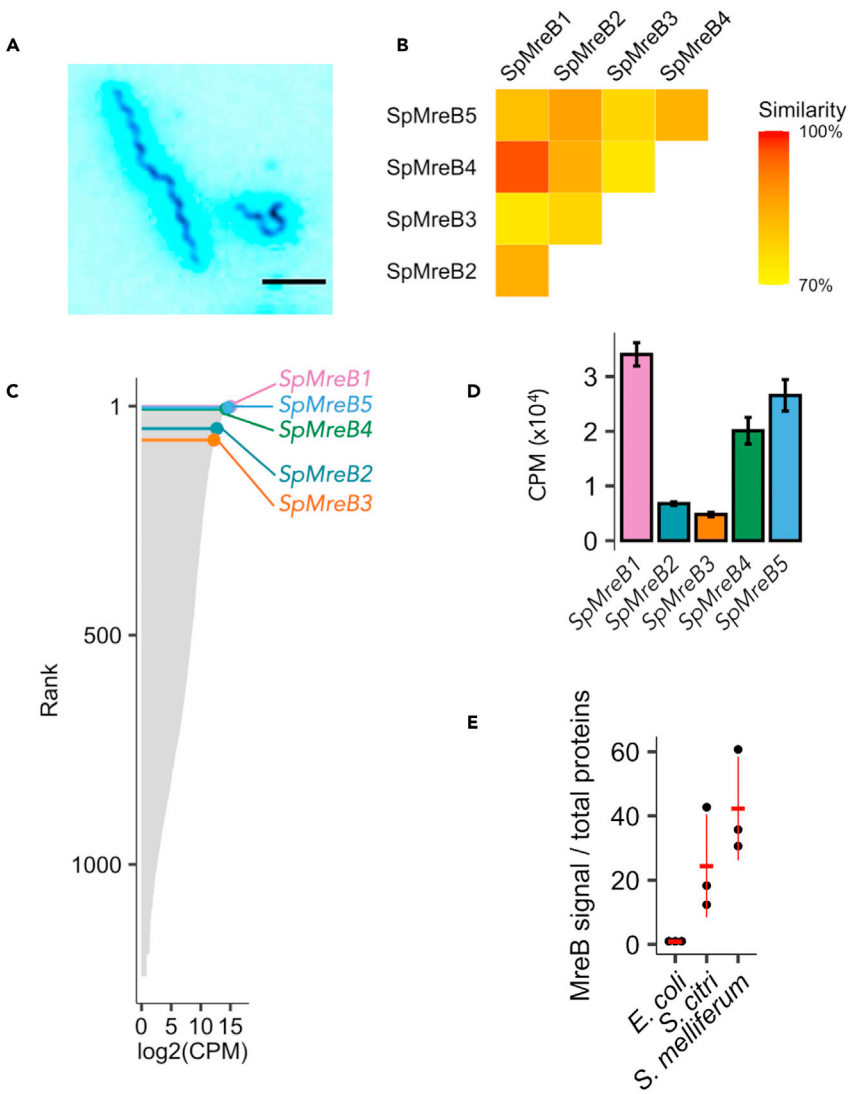

Figure 1. *Spiroplasma*MreBs are all strongly expressed *in vivo*

(A) Representative picture of *Spiroplasma poulsonii* grown *in vitro*. Scale bar = 5 μm.

(B) Matrix of the percentage of similarity between SpMreBs protein sequences. Similarity was calculated using Geneious proprietary alignment algorithm and BLOSUM45 scoring matrix.

(C) Relative expression of *SpMreB*s compared to *S. poulsonii* transcriptome. Gray bars indicate all 1491 transcripts ranked from the most to the least expressed. Lollipops indicate the position of each *SpMreBs,* in the top 5% of most expressed genes.

(D) Expression level of each isoform, in counts per million (CPM) from (Masson et al., 2018). Data are represented as mean ± SEM. (E) Western blot quantification of MreB in *E. coli*, *S. citri*, and *S. melliferum*. MreB signal was normalized to the total amount of proteins on each track as revealed by Coomassie blue staining. *Spiroplasma* ratios were normalized to 1 on the *E. coli* ratio. Each black dot represents the quantification on an independent biological replicate; the red bars and segments indicate the mean ± SEM.

shape (Townsend et al., 1980). A proteomic analysis of purified ribbons confirmed the massive presence of Fib, but also revealed the presence of MreB, a bacterial homologue of the eukaryotic actin (Bork et al., 1992; Trachtenberg et al., 2008; van den Ent et al., 2001), indicating it could play a role in maintaining *Spiroplasma's* helical shape.

MreB plays an essential function in determining the shape of almost all non-spherical bacteria (Shi et al., 2018; Wagstaff and Löwe, 2018). MreB polymerizes in an ATP-dependent fashion to form anti-parallel

double filaments that interact with the cytoplasmic tail of the transmembrane protein RodZ (Bendezú et al., 2009; van den Ent et al., 2014, 2010). The periplasmic part of RodZ then interacts with the cell wall synthesis machinery, thus linking the cell wall expansion sites (hence cell elongation) to the MreB subcellular localization (Morgenstein et al., 2015). Early studies indicated that MreB forms filaments spanning the cell length (Jones et al., 2001; Shih et al., 2003), crystallizing a hypothesis wherein MreB is a cytoskeletal protein, providing mechanical support to the cell envelope. Despite mechanical characterization that was consistent with this hypothesis, subsequent experiments suspected that these filaments were artifactual (Swulius et al., 2011; Swulius and Jensen, 2012; van den Ent et al., 2014). Fluorescent protein fusions with improved functionality and limited artifacts have helped demonstrate that MreB forms short polymers in close interaction with the membrane. These filaments undergo a processive circumferential movement around the cell as they coordinate the synthesis of new peptidoglycan (Domínguez-Escobar et al., 2011; Errington, 2015; Garner et al., 2011; Salje et al., 2011; van Teeffelen et al., 2011). In *Escherichia coli*, MreB forms filaments of varying length (most often ranging between 100 and 200 nm, and up to over 1 μm in rarer cases), too short to mechanically support the cell envelope and constitute a cell wall. Helical filaments were however observed in other fusions in *B. subtilis* and *E. coli*, reviving the helix model (Errington, 2015; Reimold et al., 2013). These conflicting localization data could however be partially explained by variations between strains or observation protocols (Errington, 2015). In summary, MreB polymers maintain cell shape indirectly by participating in the organization of the cell wall synthesis machinery, and not by directly bearing load as would be expected for a cytoskeletal protein.

Consistent with MreB's function in cell wall patterning, non-*Spiroplasma* members of the wall-less Mollicutes family lost *mreB* (Ku et al., 2014). In striking contrast, *Spiroplasma* not only retained but also multiplicated *mreB* to reach five to eight copies per genome depending on the species (Harne et al., 2020; Takahashi et al., 2020). This suggests that the protein has a major alternative function in *Spiroplasma* physiology, evidently independent of cell wall synthesis (Ku et al., 2014; Takahashi et al., 2020). A breakthrough in understanding *Spiroplasma* MreBs function has been achieved in the plant pathogenic species *Spiroplasma citri* (Harne et al., 2020). Sequencing of the naturally non-helical strain ASP-I isolated in 1980 revealed a truncation in the mreB5 gene, while *fib* and other *mreB* isoforms were intact (Townsend et al., 1980). MreB5 forms short filaments *in vitro* and can interact both with the major cytoskeleton protein Fib and with liposomes. *mreB5* deletion mutants lose their helical shape and consequently their motility (Harne et al., 2020). These observations are consistent with a scenario where MreB5 participates in maintaining *Spiroplasma* shape. However, the mechanism by which MreB5 maintains shape and the functions for the other four *mreB* paralogs still remain unknown.

Here, we investigate *Spiroplasma* MreBs functions and interactions using *Spiroplasma poulsonii*, a close relative of *S. citri* that is a natural endosymbiont of *Drosophila melanogaster* (Mateos et al., 2006). *S. poulsonii* lives in the fly hemolymph (a functional equivalent of mammal blood) and gets vertically transmitted over generations by infecting oocytes during oogenesis (Herren et al., 2013). *S. poulsonii* causes a male-killing phenotype whereby all male embryos are killed by the action of a secreted toxin, hence biasing the population toward females (Harumoto and Lemaitre, 2018). *S. poulsonii* is an interesting model to investigate the selective effect of bacterial shape because of its rapid evolution and selection through vertical transmission, which points to strong selective pressure for helical shape *in vivo* (Gerth et al., 2021). *Spiroplasma* in general are however poorly tractable bacteria *in vitro* (Masson and Lemaitre, 2020). Although some gene inactivation attempts were successful in *S. citri* (Duret et al., 1999, 2005), this genus is characterized by an extremely inefficient recombination machinery owing to the pseudogenization of *recA* (Marais et al., 1996; Masson et al., 2018; Paredes et al., 2015), which is a major hurdle for genetic engineering. *S. poulsonii* especially has only been recently cultured *in vitro* (Masson et al., 2018) and transformed to express a fluorescent marker (Masson et al., 2020), but no genomic modification has been achieved so far in this species, thus preventing a systematic knockout approach.

To explore the function of MreBs in *S. poulsonii*, we setup a heterologous expression of *Spiroplasma* MreB coding genes in *E. coli*. By individually expressing the three isoforms, we showed that each is able to polymerize in its own filamentous pattern. By systematically co-expressing isoforms in all possible combinations, we found that they together form a complex network of interactions regulating each other's polymerization patterns, which potentially determines MreBs assembly in *Spiroplasma*. In the light of these results, we propose a model of MreBs interactions and discuss why five different isoforms would be necessary to maintain morphology and motility in *Spiroplasma*.

RESULTS

Spiroplasma strongly expresses MreBs

S. poulsonii possesses five *mreB* paralogues distributed on three chromosomal loci (Masson et al., 2018; Takahashi et al., 2020). *S. poulsonii* MreBs (SpMreBs) have a remarkably high level of sequence similarity with one another (*i.e.* an identical amino acid or an amino acid with similar chemical properties at a given position), ranging between 73% for the SpMreB1-SpMreB3 comparison and 96% for the SpMreB1-SpMreB4 comparison (Figure 1B). We inspected the transcriptome of *S. poulsonii* in axenic liquid cultures for the expression levels of MreB. In these conditions, *S. poulsonii* maintains its characteristic helical shape as the one it exhibits *in vivo*. Transcriptomics data indicate that all five isoforms are expressed at high level, ranking among the top 5% of most expressed genes in *S. poulsonii* (Figure 1C) (Masson et al., 2018). Among them, *SpMreB1*, *4*, and *5* have a higher expression level than *SpMreB2* and *3* (Figure 1D). This suggests that SpMreB1, 4, and 5 are more abundant than 2 and 3. We thus explored MreB protein levels in Spiroplasmas. While we could not confirm this for *S. poulsonii* owing to the lack of cross-reactivity of anti-MreB antibodies, western blots on proteins from *S. citri* and *S. melliferum*, two other *Spiroplasma* species, show that the ratio of MreB-specific signal over total proteins was 20- to 40-fold higher than in *E. coli* (Figure 1E). This demonstrates that MreB represents a massive part of the *Spiroplasma* proteome compared with that of *E. coli*. Our transcriptome data along with the relative abundance of MreB in related *Spiroplasma* species altogether indicate that all SpMreB isoforms are strongly expressed in *S. poulsonii*.

SpMreBs form long filaments

Functional domains such as intra- and inter-protofilament binding domains and the ATP-catalytic pocket are conserved between SpMreBs and MreBs from rod-shape bacteria, which suggests that SpMreBs can form polymers (Figure S1)(Takahashi et al., 2020). We hence hypothesized that MreBs in *Spiroplasma* could play an architectural function that is the high SpMreB concentration would play a role in the formation of intracellular cytoskeletal structure that could participate in shaping *Spiroplasma* cells.

We therefore investigated the polymerization behavior of individual SpMreBs. As expected from their evolutionary history (Harne et al., 2020), SpMreB4 and SpMreB5 are highly similar to SpMreB1 and SpMreB2 (96% and 86.4%, respectively). We therefore focused on SpMreB1, 2, and 3. We circumvented the weak genetic tractability of *Spiroplasmas* by resorting to the heterologous expression of fluorescently tagged SpMreB in *E. coli* cells. Heterologous expression has been instrumental in investigation of MreB structure and dynamics (Chiu et al., 2008; Srinivasan et al., 2007). Here, we built a sandwich fusion where the coding sequence for a monomeric superfolder green fluorescent protein (GFP) is inserted on a poorly conserved external loop, generating a functional MreB fusion with limited alterations of its native structure (Bendezú et al., 2009; Ouzounov et al., 2016; Swulius and Jensen, 2012; Ursell et al., 2014). The sandwich fusion to the native *E. coli* MreB (EcMreB^{GFP}) displayed the characteristic peripheral diffraction-limited puncta pattern along the membrane (Swulius and Jensen, 2012) (Figures 2Aand S2). In contrast, the three SpMreB^{GFP} isoforms formed distinctive filament-like structures when expressed at high levels as in *Spiroplasmas*. SpMreB1^{GFP} formed filaments a few micrometer-long extending along the cell. SpMreB2^{GFP} formed long and thick filaments along the cell, which connected large puncta. The puncta resemble inclusion bodies and could either be a SpMreB2 proper structure or protein aggregates owing to overexpression, although their appearance at low induction levels rather points to the former hypothesis. SpMreB3 mainly formed transverse filaments forming ring-like structures across the cell (Figures 2A and S2).

We assessed the robustness of our heterologous expression approach by investigating the interaction of our constructs with the native MreB of *E. coli*. We showed that a ΔmreB mutant strain (Shi et al., 2017) cannot be complemented with an untagged version of SpMreB1, as expected (Figure S3A). Previous studies showed that altering EcMreB polymerization causes shape defects (Shi et al., 2018); we therefore co-expressed EcMreB and SpMreB1 in the ΔmreB strain. We did not observe any growth or shape defect upon co-expression with increasing levels of SpMreB1 (Figures S3B and S3C), which suggests that it does not interfere with EcMreB. SpMreBs also had little effect on the cell's morphology, although they appeared slightly elongated upon SpMreB1 and SpMreB2 expression and slightly thinner or wider upon expression of SpMreB1 or SpMreB2 and 3, respectively (Figures S3D and S3E). Furthermore, immunofluorescence on native EcMreB indicated that the peripheral puncta pattern was not disrupted upon expression of SpMreB1, 2, or 3 (Figure S3F). Last, we tested if SpMreB isoforms can interact with EcMreB using a bacterial two-hybrid approach based on the reconstitution of the adenylate cyclase of *E. coli* upon protein–protein

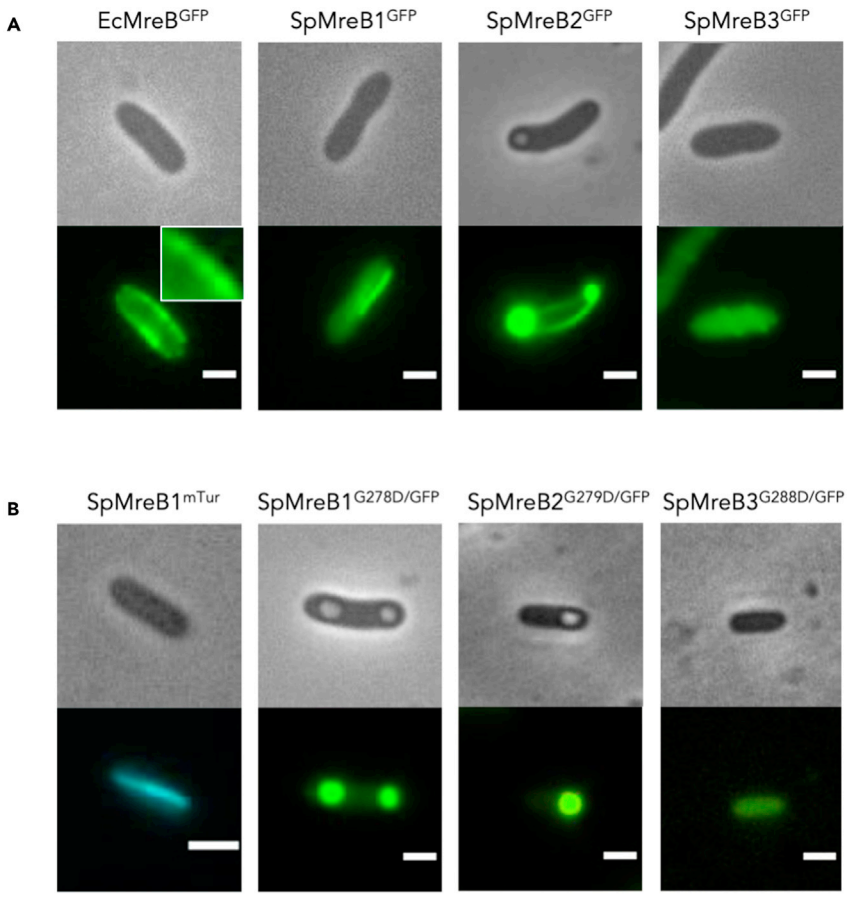

Figure 2. SpMreBs form filaments when expressed in *E. coli* cells

(A) *E. coli* cell expressing MreB^{GFP} constructs. The typical peripheral puncta along the membrane are observed with EcMreB^{GFP} (inset is a 2X magnification), SpMreB1^{GFP} shows longitudinal filaments; SpMreB2^{GFP} shows pole puncta and longitudinal filament; SpMreB3^{GFP} shows transversal filaments.

(B) *E. coli* cells expression SpMreB1^{mTur2} showing similar longitudinal filaments to that formed by SpMreB1^{GFP}; or expressing the point-mutated constructs SpMreB1$^{G278D/GFP}$, SpMreB2$^{G279D/GFP}$, and SpMreB3$^{G288D/GFP}$ (mutation on the intrafilament interaction region). Scale bar = 2 μm.

interaction (BACTH) (Karimova et al., 1998). Pairwise comparison of EcMreB with SpMreB1, 2, or 3 revealed no signal, further indicating that SpMreBs do not interact with EcMreB (Figure S3G).

MreB fusions are prone to artifactual polymerization, in particular at high expression levels (Swulius and Jensen, 2012). To control potential artifacts, we generated SpMreBs point mutants in the intrafilament interaction region and visualized polymerization phenotypes (Takahashi et al., 2020; van den Ent et al., 2014) (Figure S1). None of the SpMreB1$^{G278D/GFP}$, SpMreB2$^{G279D/GFP}$, and SpMreB3$^{G288D/GFP}$ mutants formed filaments. Instead, these mutants showed either accumulated signal in puncta or displayed no signal (Figure 2B), indicating that wild-type constructs formed polymers that are unlikely to be artifactual or aggregates of misfolded proteins. Consistent with this, we could observe filaments similar to SpMreB1^{GFP} when swapping GFP to the fluorescent protein mTurquoise2 (Figure 2B). Finally, we visualized native EcMreB in SpMreB-expressing *E. coli* by immunofluorescence. We could not observe any misshaping or change in localization pattern of EcMreB, which indicates that there are no confounding interactions between SpMreBs and the native EcMreB (supplemental information Text and Figures S3A–S3F).

We then looked into the mechanism of filament formation. We hypothesized that protein–protein interactions between SpMreBs drive the formation of polymers. To test this hypothesis, we measured the interaction of each isoform with itself using the BACTH two-hybrid system (Figure S3G). We observed a strong

BACTH signal for all isoforms indicating that each SpMreB interact with themselves, which likely leads to polymerization and filament formation observed in Figure 2A.

Spiroplasma MreB filaments are polymorphic and dynamic

Remarkably, while fluorescent EcMreB gave a consistent pattern from one cell to another, SpMreB^{GFP}-expressing cells had an important phenotypic heterogeneity. We thus carefully categorized the morphology of the filaments formed by single-isoform SpMreB^{GFP} in the heterologous expression system. Most cells formed filaments (Figure 3A). Quantitative analysis revealed that the filament patterns shown in Figure 2A are isoform-specific: longitudinal filaments are proper to SpMreB1^{GFP}, puncta associated with filaments proper to SpMreB2^{GFP} and transversal filaments proper to SpMreB3^{GFP} (Figure 3A). We found that for all isoforms, only a small proportion of cells had a homogenously diffused cytoplasmic signal. In addition, only a small proportion of cells displayed puncta without filaments in SpMreB2 and 3.

Increasing the induction level of the SpMreB1^{GFP} construct to 1 mM IPTG (a concentration commonly used for recombinant protein production) leads to swollen, round cells. These easily rupture upon mechanical pressure and release filaments in the vicinity of the dead cell (Figure 3B), suggesting that they are not tightly attached to the cell envelope. Overexpressing SpMreB3 did not yield any interpretable observations as most of the surviving population seemed to systematically lose fluorescence. Strongly inducing SpMreB2 with 1 mM IPTG resulted in cells with consistently aberrant shapes, accompanied with puncta accumulation and swelling (Figure 3B). We occasionally observed strings of normally shaped cells connected by a continuous SpMreB2 filament (Figure 3C). This could be the result of the inability of *E. coli* to cut the filament transversally during division; hence, the structure is extending from between two daughters, blocking their separation.

EcMreb filament processivity drives a net movement of filaments along the cell. We therefore wondered whether SpMreB was also mobile. We thus performed dynamics visualization of the SpMreB1, 2, and 3 filaments by time-lapse microscopy in our heterologous system. Visualizations of SpMreB1 and SpMreB3 filaments more than two hours did not resolve any mobility during or after polymerization. In contrast, SpMreB2 filaments were dynamic after completion (Figures 3D and 3E and Videos S2 and S3). Specifically, we observed multiple filaments undergoing lateral displacements. When cells had several filaments, they merged into thicker bundles, generally associated along the cell envelope (Figure 3D andVideo S2). These data allowed us to estimate that SpMreB2 protofilaments move at a rather slow speed within *E. coli* cells, ranging from 30 to 60 nm/min. For comparison, EcMreB filaments move at 1 to 5 μm/min (Reimold et al., 2013).

SpMreBs form an interaction network *in vivo*

Cryo-electron tomography performed on *Spiroplasma melliferum* cells has provided an empirical basis for the ultrastructure of the *Spiroplasma* cytoskeleton. Two models were inferred from these tomograms. The first model (three-ribbon model) proposes that the cytoskeleton is composed of a ribbon of thin filaments (presumably formed by MreBs) sandwiched between two ribbons of thicker filaments (presumably formed by fibril proteins) (Kürner et al., 2005). Alternatively, the second model (one-ribbon model) proposes that a single ribbon composed of mingled Fib and MreBs forms the cytoskeleton (Trachtenberg et al., 2008). In both models, however, the cytoskeleton is only composed of one or two filament types. Therefore, the five polymer-forming MreBs and Fib that compose the filaments are very likely to interact with one another.

To identify the potential interactions between SpMreB isoforms, we first employed a high throughput approach and performed co-immunoprecipitation (co-IP). We overexpressed and purified single SpMreBs^{GFP} and incubated them with a total protein extract of wild-type *S. poulsonii*. Complexes formed between the SpMreBs^{GFP} fusion proteins and native *S. poulsonii* were then purified, broken down, and their components were analyzed by mass spectrometry (LC-MS/MS). This approach identified 231 *S. poulsonii* proteins interacting with at least one SpMreB isoform. Remarkably, each isoform had at least one other isoform among its interactors, indicating that they most likely all act in combination *in vivo* to build the *Spiroplasma* cytoskeleton (Figure S4). We thus identified the direct interaction network between isoforms (Data S1 and Figure S4). Only SpMreB1 interacts with Fib, suggesting that it could serve in anchoring the SpMreBs structure to the Fib ribbon. As this co-IP analysis suggests *in vivo* interactions between isoforms, we went on to test specific interactions between each isoform and their effect on the regulation of polymerization.

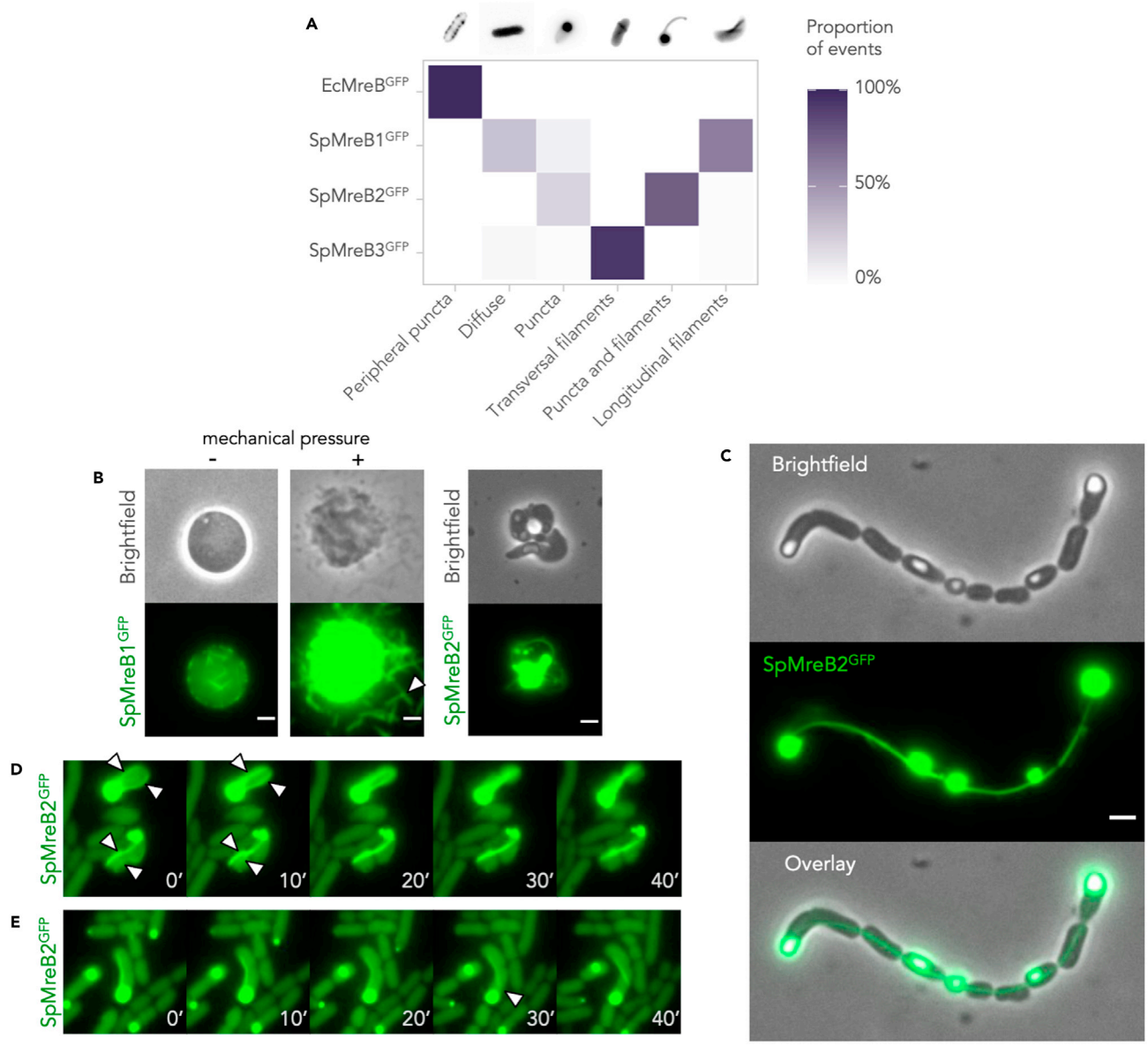

Figure 3. SpMreBs have distinct filament pattern and dynamics

(A) Identification of the main filament patterns and quantification of their observed proportion upon expression of single MreB^{GFP} construct. Color density indicates a percentage of observations for each condition, from n > 250 observations from three independent replicates.

(B) SpMreB^{GFP} upon strong induction (1 mM IPTG) showing cell rounding for SpMreB1^{GFP} and release of the filaments in the close environment upon mechanical cell lysis and cell misshaping for SpMreB2^{GFP}.

(C) Overexpression of SpMreB2^{GFP} resulting in a string of cells connected by a thick filament.

(D) Timelapse of SpMreB2^{GFP} protofilament fusion. White arrows show the protofilaments before their merging.

(E) Timelapse of a SpMreB2^{GFP} filament detaching from a punctum. The white arrow indicates the moment and location when the filament detaches. Times from the first pictures are indicated on each sub-panel in minutes. Scale bars = 2 μm.

The SpMreBs interaction network orchestrates polymerization

We then investigated whether the inter-SpMreBs interactions identified by co-IP could regulate their polymerization and filament formation. We thus simultaneously expressed several isoforms in *E. coli* and visualized the resulting polymerization patterns, which we could then compare with single isoform expression (Figure 2).

To rigorously delineate the function for the SpMreB interaction network, we therefore used a combinatorial approach based on the observation of a single-tagged isoform co-expressed with untagged isoforms. For

simplicity, we named these combinations using only their isoform numbers with a superscript "GFP" directly following the number of the tagged isoform (*e.g.* 1^{GFP}-23 refers to the construct SpMreB1^{GFP}-SpMreB2-SpMreB3; see Figure S5). If all isoforms are part of a single structure, we should observe similar fluorescence patterns independent of the GFP tag position. This was the case for SpMreB1 and SpMreB3 as indicated by the identical pattern of 1^{GFP}-23 and 123^{GFP}, for which we both observed cells with longitudinal filaments and cells with puncta and longitudinal filaments in similar proportions (Figure 4A). SpMreB2 in 12^{GFP}-3 however displayed a diffuse phenotype, distinct from the other two combinations, and also different from its single expression. This confirms that SpMreB filaments do not simply form a single structure but rather act through an elaborate interaction network regulating filament formation.

To further characterize how interactions between isoforms regulate filament formation, we turned to co-expression of SpMreB pairs. The proportion of longitudinal filaments observed in the single 1^{GFP} expression was lower in 1^{GFP}-3 and 1^{GFP}-23, but remained at single expression levels in in 1^{GFP}-2. This indicates that SpMreB3 modulates SpMreB1 polymerization (Figure 4B) while SpMreB2 has little to no effect on SpMreB1. Co-expression, where the GFP tag is on SpMreB3 gave a more complex phenotype. Transversal filaments were observed in almost all cells upon SpMreB3^{GFP} single-expression (Figures 2A and 3A), while none of these filaments were detected with the 123^{GFP} construct (Figure 4A). This indicates that the presence of both SpMreB1 and SpMreB2 inhibits SpMreB3 transversal filament formation. However, such transversal filaments were observed with both the 13^{GFP} and 23^{GFP} constructs (Figure 4B), indicating that SpMreB1 and SpMreB2 must be both present to completely inhibit their formation. The proportion of cells harboring transversal filaments was higher upon 23^{GFP} expression (44% on average) than 13^{GFP} expression (10% on average), indicating a stronger inhibition from SpMreB1 than from SpMreB2. Collectively, this indicates that SpMreB1 and SpMreB3 form filaments together while having a limiting effect on each other's polymerization.

12^{GFP}-3 on the other hand had its proper pattern with a majority of cells displaying a diffuse cytoplasmic signal and a few harboring puncta (Figure 4A). This phenotype is independent of the order of transcription of the isoforms which may affect stoichiometry, as it is identical to that observed with a 2^{GFP}-31 construct (Figure 4B) (Lim et al., 2011). This suggests that SpMreB1 and/or SpMreB3 inhibit SpMreB2 filament formation. Both 2^{GFP}-3 and 12^{GFP} displayed similar results to 12^{GFP}-3, indicating that the presence of any of the other isoforms can inhibit SpMreB2 filament structuring (Figure 4B).

DISCUSSION

The conservation and duplications of MreB coding genes in *Spiroplasma* raise major questions regarding their function in wall-less bacteria (Ku et al., 2014; Takahashi et al., 2020). Here, we report evidence supporting that all SpMreBs isoforms are able to form filaments *in vivo* and that each isoform can affect the polymerization pattern of others through a complex network of interactions. As a consequence, this suggests that [SpMreB1-SpMreB4],[SpMreB2-SpMreB5], and [SpMreB3] clusters have distinct functions and are not necessarily redundant. From our observations, we can infer the existence of at least two separate structures upon heterologous expression in *E. coli*, one involving SpMreB1 (and possibly the closest homolog, SpMreB4) with SpMreB3 and one involving SpMreB2 (and possibly the closest homolog, SpMreB5). Yet, we uncovered interaction between almost all isoforms in the co-immunoprecipitation experiment, suggesting that although polymeric structures are distinct, the monomers themselves are probably able to interact with one another.

SpMreB1 formed static filament structures that do not attach to the cell envelope (Figures 2A and 3B). We thus hypothesize that it could form a backbone structure on which other isoforms would associate. Its interaction with Fib suggests a potential association with the Fib ribbon, hence coordinating Fib and MreB functions. Interestingly, SpMreB3 was the only isoform producing transversal filaments, similar to the orientation of EcMreB polymers. Furthermore, an amphipathic helix has been predicted on the N-terminus region of *Spiroplasma* MreB3s (Takahashi et al., 2020), suggesting an ability to attach to membranes. The *S. citri* ASP-I mutant that has intact MreB1 and MreB3 isoforms is not helical, which indicates that SpMreB3 is not sufficient to form helical cells (Harne et al., 2020). SpMreB3 could instead serve as a set attachment point between filaments formed by other isoforms and the membrane and twist them to follow the cell body helicity maintained by SpMreB5 (and possibly SpMreB2).

Spiroplasma swims by changing shape. Cells deform their membrane by producing a kink in their helix. The propagation of this kink along the cell body propels the cell forward. Kinks are produced by a local and

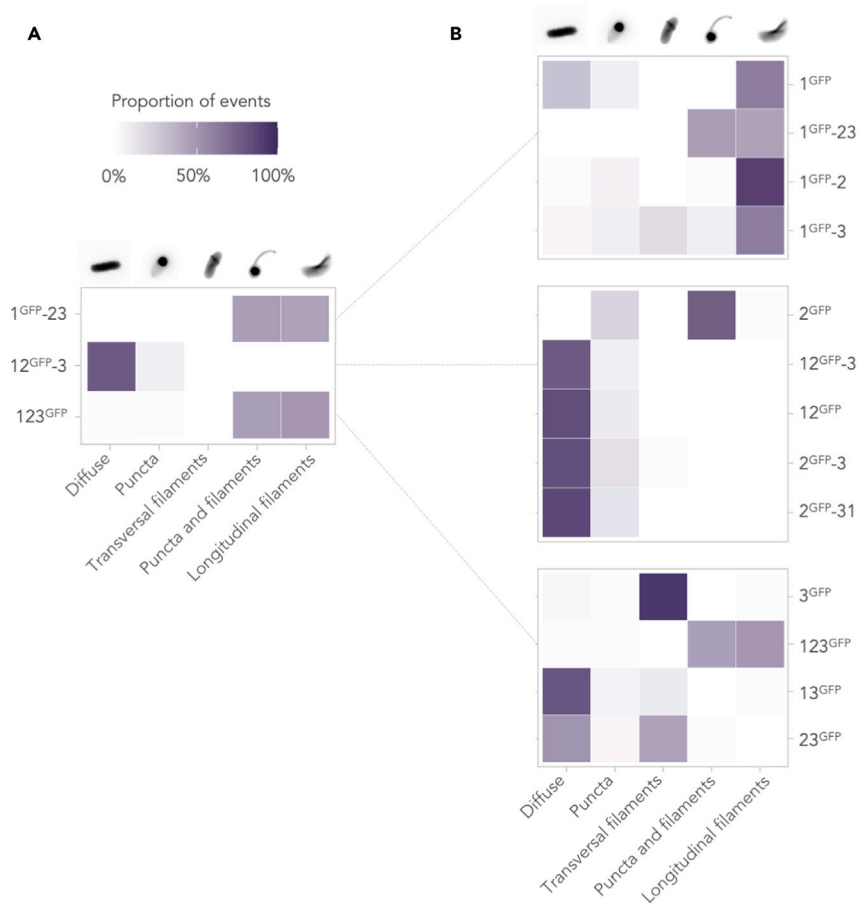

Figure 4. SpMreB interactions regulate polymerization

(A and B) Identification of the main patterns and quantification of their proportion upon expression of transcriptional fusion construct with the GFP tag on SpMreB1, SpMreB2, or SpMreB3. Color density indicates a percentage of observations for each condition, from n > 250 observations from three independent replicates.

processive change in the cell body helicity (Shaevitz et al., 2005), but the exact mechanism regulating helicity and handedness is still elusive. We suspect that active motion of MreB and Fib filaments relative to each other can produce these deformations. We found that SpMreB2, the closest homolog *S. citri* MreB5 (Harne et al., 2020), was the only isoform producing mobile filaments. A proposed model based on a single-ribbon cytoskeleton involves a coordinated length change of the filaments forming the internal ribbon, with unknown proteins anchoring the moving fibrils to the membrane to propagate movement to the cell (Berg, 2002; Trachtenberg and Gilad, 2001). In the three-ribbon cytoskeletal model, the shortening of one ribbon would be sufficient to cause a change in the helix handedness, resulting in the formation of the kink (Kürner et al., 2005). In this case, only one ribbon needs to be mobile while others could stay fixed and serve as an anchoring point. SpMreB2 polymerization pattern involved large puncta and filaments that are connected to the puncta but are also attached to the cell body on their own (see Figures 3A and 3C). The puncta themselves could serve as attachment structures as their localization seems to be defined at the cell pole or more rarely at the cell center. SpMreB2 filaments could directly attach to the membrane since the homologous MreB5 can interact with liposomes (Harne et al., 2020). Taken together, the mobility and attachment features of SpMreB2 make it a promising candidate as a regulator of *Spiroplasma* motility. An attractive hypothesis would be that [SpMreB1-SpMreB3] (and possibly SpMreB4) form fixed structures anchored to the membrane (by SpMreB3 and the Fib ribbon (by SpMreB1), against which the [SpMreB2-SpMreB5] structure slides to produce and propagate the kinks.

Last, the SpMreB2 filaments grew into long and mechanically robust filaments upon overexpression of the single construct that are deleterious to *E. coli* growth. We hypothesize that a *Spiroplasma*-specific

mechanism regulates SpMreB2 filament length in native conditions. This mechanism could involve a yet uncharacterized protein capable of cutting the filament or limiting its growth (possibly another SpMreB isoform). Alternatively, filament bundles could be split longitudinally during cell division (yielding back the thinner filaments observed before bundling or merging), which would be in accordance with the remarkable division process of the bacterium whereby cells split longitudinally (Ramond et al., 2016).

Collectively, our results support the hypothesis of a sub-functionalization of each isoform, which could build a complex polymeric inner structure by interacting with one another. Despite rigorous mechanical characterization experiments that highlight a load-bearing function of MreB in *E. coli* (Wang et al., 2010), the hypothesis where MreB filaments provide mechanical stability has been largely abandoned, favoring a model where MreB almost exclusively functions by patterning the cell wall. The high abundance of SpMreB isoforms *in vivo*, as well as the high induction level required to observe filaments in our heterologous system, is rather reminiscent of eukaryotic actin. To form a robust cytoskeleton, mammalian cells must maintain a high concentration of intracellular actin monomer to maintain polymerization, making actin one of the most highly expressed proteins in a cell. In the light of our data and of *Spiroplasma* biology, we propose that the MreB polymeric structure could coordinate the Fib cytoskeleton and the membrane to maintain *Spiroplasma* helicity and generate kink movement. The example of *Spiroplasma* MreBs highlights the divergent evolution of these proteins in wall-less bacteria, where they control bacterial shape through mechanisms that are independent of peptidoglycan synthesis.

Limitations of the study

Heterologous expression studies can produce useful insights into the respective functions of SpMreBs and their interactions. However, it is subject to biases owing to the protein tagging, the presence of *E. coli* proteins that can interact with them, or the lack of interactors that regulate filament formation in *Spiroplasma* cells. The development of genetic tools in *S. poulsonii* will hence be required for a definitive confirmation of the role and sub-functionalization of SpMreB isoforms *in vivo*.

STAR★METHODS

Detailed methods are provided in the online version of this paper and include the following:

- KEY RESOURCES TABLE
- RESOURCE AVAILABILITY
  - Lead contact
  - Materials availability
  - Data and code availability
- EXPERIMENTAL MODEL AND SUBJECT DETAILS
- METHODS DETAILS
  - Genetic constructs
  - Sequence analysis and alignment
  - Live fluorescence microcopy
  - Immunofluorescence microcopy
  - Western Blot
  - Growth curves
  - Morphology measurements
  - Bacterial two-hybrid assay
  - Sample preparation for co-immunoprecipitation
  - Co-immunoprecipitation
  - LC-MS/MS and data analysis
- QUANTIFICATION AND STATISTICAL ANALYSIS
  - Softwares
  - Quantitative filament analysis
  - Morphology measurements
  - Co-immunoprecipitation data analysis

SUPPLEMENTAL INFORMATION

Supplemental information can be found online at https://doi.org/10.1016/j.isci.2021.103458.

ACKNOWLEDGMENTS

We are grateful to Rut Carballido-López, Yuko Inclan, Nikolay Ouzounov, Alice Cont, Handuo Shi, and Kerwyn Casey Huang for providing critical reagents and plasmids.

This work was supported in part using the resources and services of the Proteomics Research Core Facility at the School of Life Sciences of EPFL and we are especially grateful to Romain Hamelin and Florence Armand for their input on the co-immunoprecipitation experiment.

This work was funded by the Swiss National Science Foundation grants N310030_185295 and 189084, the Human Frontiers Science Program RGY0077 and the Giorgi Cavaglieri Foundation.

AUTHOR CONTRIBUTIONS

FM and AP designed research; FM and XP performed research; FM analyzed data; AP and BL supervised the project; FM and AP wrote the manuscript. All authors contributed to the manuscript editing and validated the final version.

DECLARATION OF INTERESTS

The authors declare no competing interests.

Received: October 8, 2021
Revised: November 3, 2021
Accepted: November 11, 2021
Published: December 17, 2021

REFERENCES

Bendezú, F.O., Hale, C.A., Bernhardt, T.G., and de Boer, P.A.J. (2009). RodZ (YfgA) is required for proper assembly of the MreB actin cytoskeleton and cell shape in E. coli. EMBO J. *28*, 193–204. https://doi.org/10.1038/emboj.2008.264.

Berg, H.C. (2002). How Spiroplasma might swim. J. Bacteriol. *184*, 2063 LP–2064. https://doi.org/10.1128/JB.184.8.2063-2064.2002.

Billings, G., Ouzounov, N., Ursell, T., Desmarais, S.M., Shaevitz, J., Gitai, Z., and Huang, K.C. (2014). De novo morphogenesis in L-forms via geometric control of cell growth. Mol. Microbiol. *93*, 883–896. https://doi.org/10.1111/mmi.12703.

Bork, P., Sander, C., and Valencia, A. (1992). An ATPase domain common to prokaryotic cell cycle proteins, sugar kinases, actin, and hsp70 heat shock proteins. Proc. Natl. Acad. Sci. U S A *89*, 7290–7294. https://doi.org/10.1073/pnas.89.16.7290.

Bové, J.M. (1993). Molecular features of mollicutes. Clin. Infect.Dis. *17*, S10–S31.

Cabeen, M.T., and Jacobs-Wagner, C. (2005). Bacterial cell shape. Nat. Rev. Microbiol. *3*, 601.

Chiu, S., Chen, S., and Wong, H. (2008). Dynamic localization of MreB in Vibrio parahaemolyticus and in the ectopic host bacterium Escherichia coli. Appl.Environ.Microbiol. *74*, 6739–6745. https://doi.org/10.1128/AEM.01021-08.

Cox, J., Hein, M.Y., Luber, C.A., Paron, I., Nagaraj, N., and Mann, M. (2014). Accurate proteome-wide label-free quantification by delayed normalization and maximal peptide ratio extraction, termed MaxLFQ. Mol. Cell Proteom. *13*, 2513–2526. https://doi.org/10.1074/mcp.M113.031591.

Cox, J., and Mann, M. (2008). MaxQuant enables high peptide identification rates, individualized p.p.b.-range mass accuracies and proteome-wide protein quantification. Nat. Biotechnol. *26*, 1367–1372. https://doi.org/10.1038/nbt.1511.

Domínguez-Escobar, J., Chastanet, A., Crevenna, A.H., Fromion, V., Wedlich-Söldner, R., and Carballido-López, R. (2011). Processive movement of MreB-associated cell wall biosynthetic complexes in bacteria. Science *333*, 225–228. https://doi.org/10.1126/science.1203466.

Dorin-Semblat, D., Demarta-Gatsi, C., Hamelin, R., Armand, F., Carvalho, T.G., Moniatte, M., and Doerig, C. (2015). Malaria parasite-infected erythrocytes secrete PfCK1, the plasmodium homologue of the pleiotropic protein kinase casein kinase 1. PLoS One *10*, e0139591.

Duret, S., André, A., and Renaudin, J. (2005). Specific gene targeting in Spiroplasma citri: improved vectors and production of unmarked mutations using site-specific recombination. Microbiology *151*, 2793–2803. https://doi.org/10.1099/mic.0.28123-0.

Duret, S., Danet, J.-L., Garnier, M., and Renaudin, J. (1999). Gene disruption through homologous recombination in Spiroplasma citri: an scm1-disrupted motility mutant is pathogenic. J. Bacteriol. *181*, 7449–7456.

Errington, J. (2015). Bacterial morphogenesis and the enigmatic MreB helix. Nat. Rev. Microbiol. *13*, 241–248. https://doi.org/10.1038/nrmicro3398.

Garner, E.C., Bernard, R., Wang, W., Zhuang, X., Rudner, D.Z., and Mitchison, T. (2011). Coupled, circumferential motions of the cell wall synthesis machinery and MreB filaments in B. subtilis. Science *333*, 222–225. https://doi.org/10.1126/science.1203285.

Gasparich, G.E. (2002). Spiroplasmas: evolution, adaptation and diversity. Front. Biosci. *7*, 619–640.

Gerth, M., Montoya, H.M., Ramirez, P., Masson, F., Griffin, J.S., Aramayo, R., Siozios, S., Lemaitre, B., Mateos, M., and Hurst, G.D.D. (2021). Rapid molecular evolution of Spiroplasma symbionts of Drosophila. Microb.Genom. *7*, 000503. https://doi.org/10.1099/mgen.0.000503.

Harne, S., Duret, S., Pande, V., Bapat, M., Béven, L., and Gayathri, P. (2020). MreB5 is a determinant of rod-to-helical transition in the cell-wall-less bacterium Spiroplasma. Curr.Biol. *30*, 4753–4762.e7. https://doi.org/10.1016/j.cub.2020.08.093.

Hartmann, R., van Teeseling, M.C.F., Thanbichler, M., and Drescher, K. (2020). BacStalk: a comprehensive and interactive image analysis software tool for bacterial cell biology. Mol. Microbiol. *114*, 140–150. https://doi.org/10.1111/mmi.14501.

Harumoto, T., and Lemaitre, B. (2018). Male-killing toxin in a bacterial symbiont of Drosophila. Nature *557*, 252–255. https://doi.org/10.1038/s41586-018-0086-2.

Herren, J.K., Paredes, J.C., Schüpfer, F., and Lemaitre, B. (2013). Vertical transmission of a Drosophila endosymbiont via cooption of the yolk transport and internalization machinery.

mBio *4*. e00532–12. https://doi.org/10.1128/mBio.00532-12.

Jones, L.J.F., Carballido-López, R., and Errington, J. (2001). Control of cell shape in bacteria: helical, actin-like filaments in Bacillus subtilis. Cell *104*, 913–922. https://doi.org/10.1016/S0092-8674(01)00287-2.

Karimova, G., Pidoux, J., Ullmann, A., and Ladant, D. (1998). A bacterial two-hybrid system based on a reconstituted signal transduction pathway. Proc. Natl. Acad. Sci. U S A *95*, 5752 LP–5756. https://doi.org/10.1073/pnas.95.10.5752.

Ku, C., Lo, W.-S., and Kuo, C.-H. (2014). Molecular evolution of the actin-like MreB protein gene family in wall-less bacteria. Biochem.Biophys. Res. Commun. *446*, 927–932. https://doi.org/10.1016/j.bbrc.2014.03.039.

Kürner, J., Frangakis, A.S., and Baumeister, W. (2005). Cryo–electron tomography reveals the cytoskeletal structure of Spiroplasma melliferum. Science, 436–438. https://doi.org/10.1126/science.1104031.

Kysela, D.T., Randich, A.M., Caccamo, P.D., and Brun, Y.V. (2016). Diversity takes shape: understanding the mechanistic and adaptive basis of bacterial morphology. PLoS Biol. *14*, e1002565.

Lim, H.N., Lee, Y., and Hussein, R. (2011). Fundamental relationship between operon organization and gene expression. Proc. Natl. Acad. Sci. U S A *108*, 10626–10631. https://doi.org/10.1073/pnas.1105692108.

Marais, A., Bove, J.M., and Renaudin, J. (1996). Characterization of the recA gene regions of Spiroplasma citri and Spiroplasma melliferum. J.Bacteriol. *178*, 7003–7009.

Masson, F., Calderon Copete, S., Schüpfer, F., Garcia-Arraez, G., and Lemaitre, B. (2018). In vitro culture of the insect endosymbiont Spiroplasma poulsonii highlights bacterial genes involved in host-symbiont interaction. mBio *9*. e00024–18. https://doi.org/10.1128/mBio.00024-18.

Masson, F., and Lemaitre, B. (2020). Growing ungrowable bacteria: overview and perspectives on insect symbiont culturability. Microbiol.Mol. Biol. Rev. *84*. e00089-20. https://doi.org/10.1128/MMBR.00089-20.

Masson, F., Schüpfer, F., Jollivet, C., and Lemaitre, B. (2020). Transformation of the Drosophila sex-manipulative endosymbiont Spiroplasma poulsonii and persisting hurdles for functional genetics studies. Appl. Environ.Microbiol. 00835-20. https://doi.org/10.1128/AEM.00835-20.

Mateos, M., Castrezana, S.J., Nankivell, B.J., Estes, A.M., Markow, T.A., and Moran, N.A. (2006). Heritable endosymbionts of Drosophila. Genetics *174*, 363–376.

Morgenstein, R.M., Bratton, B.P., Nguyen, J.P., Ouzounov, N., Shaevitz, J.W., and Gitai, Z. (2015). RodZ links MreB to cell wall synthesis to mediate MreB rotation and robust morphogenesis. Proc. Natl. Acad. Sci. U S A *112*, 12510–12515. https://doi.org/10.1073/pnas.1509610112.

Ouzounov, N., Nguyen, J.P., Bratton, B.P., Jacobowitz, D., Gitai, Z., and Shaevitz, J.W. (2016). MreB orientation correlates with cell diameter in Escherichia coli. Biophys. J. *111*, 1035–1043. https://doi.org/10.1016/j.bpj.2016.07.017.

Paredes, J.C., Herren, J.K., Schüpfer, F., Marin, R., Claverol, S., Kuo, C.-H., Lemaitre, B., and Béven, L. (2015). Genome sequence of the Drosophila melanogaster male-killing Spiroplasma strain MSRO endosymbiont. mBio *6*. e02437-14. https://doi.org/10.1128/mBio.02437-14.

Ramond, E., Maclachlan, C., Clerc-Rosset, S., Knott, G.W., and Lemaitre, B. (2016). Cell division by longitudinal scission in the insect endosymbiont Spiroplasma poulsonii. mBio *7*, e00881-16.

Rappsilber, J., Mann, M., and Ishihama, Y. (2007). Protocol for micro-purification, enrichment, pre-fractionation and storage of peptides for proteomics using StageTips. Nat. Protoc. *2*, 1896–1906. https://doi.org/10.1038/nprot.2007.261.

Reimold, C., Defeu Soufo, H.J., Dempwolff, F., and Graumann, P.L. (2013). Motion of variable-length MreB filaments at the bacterial cell membrane influences cell morphology. Mol. Biol.Cell *24*, 2340–2349. https://doi.org/10.1091/mbc.e12-10-0728.

Salje, J., van den Ent, F., de Boer, P., and Löwe, J. (2011). Direct membrane binding by bacterial actin MreB. Mol.Cell *43*, 478–487. https://doi.org/10.1016/j.molcel.2011.07.008.

Sasajima, Y., Kato, T., Miyata, T., Namba, K., and Miyata, M. (2021). Elucidation of fibril structure responsible for swimming in Spiroplasma using electron microscopy. bioRxiv.

Shaevitz, J.W., Lee, J.Y., and Fletcher, D.A. (2005). Spiroplasma swim by a processive change in body helicity. Cell *122*, 941–945. https://doi.org/10.1016/j.cell.2005.07.004.

Shi, H., Bratton, B.P., Gitai, Z., and Huang, K.C. (2018). How to build a bacterial cell: MreB as the foreman of E. coli construction. Cell *172*, 1294–1305. https://doi.org/10.1016/j.cell.2018.02.050.

Shi, H., Colavin, A., Bigos, M., Tropini, C., Monds, R.D., and Huang, K.C. (2017). Deep phenotypic mapping of bacterial cytoskeletal mutants reveals physiological robustness to cell size. Curr.Biol. *27*, 3419–3429.e4. https://doi.org/10.1016/j.cub.2017.09.065.

Shih, Y.-L., Le, T., and Rothfield, L. (2003). Division site selection in Escherichia coli involves dynamic redistribution of Min proteins within coiled structures that extend between the two cell poles. Proc. Natl. Acad. Sci. U S A *100*, 7865–7870. https://doi.org/10.1073/pnas.1232225100.

Srinivasan, R., Mishra, M., Murata-Hori, M., and Balasubramanian, M.K. (2007). filament formation of the Escherichia coli actin-related protein, MreB, in fission yeast. Curr. Biol. *17*, 266–272. https://doi.org/10.1016/j.cub.2006.11.069.

Svitkina, T. (2018). The actin cytoskeleton and actin-based motility. Cold Spring Harbor Perspect.Biol. *10*, a018267.

Swulius, M.T., Chen, S., Jane Ding, H., Li, Z., Briegel, A., Pilhofer, M., Tocheva, E.I., Lybarger, S.R., Johnson, T.L., Sandkvist, M., and Jensen, G.J. (2011). Long helical filaments are not seen encircling cells in electron cryotomograms of rod-shaped bacteria. Biochem.Biophys.Res.Commun. *407*, 650–655. https://doi.org/10.1016/j.bbrc.2011.03.062.

Swulius, M.T., and Jensen, G.J. (2012). The helical MreB cytoskeleton in Escherichia coli MC1000/pLE7 is an artifact of the N-terminal yellow fluorescent protein tag. J. Bacteriol. *194*, 6382–6386. https://doi.org/10.1128/JB.00505-12.

Takahashi, D., Fujiwara, I., and Miyata, M. (2020). Phylogenetic origin and sequence features of MreB from the wall-less swimming bacteria Spiroplasma. Biochem.Biophys. Res. Commun. https://doi.org/10.1016/j.bbrc.2020.09.060.

Townsend, R., Burgess, J., and Plaskitt, K.A. (1980). Morphology and ultrastructure of helical and nonhelical strains of Spiroplasma citri. J.Bacteriol. *142*, 973–981. https://doi.org/10.1128/JB.142.3.973-981.1980.

Townsend, R., and Plaskitt, K.A. (1989). Immunogoldlocalization of p55-fibril protein and p25-spiralin in Spiroplasma cells. J. Gen. Microbiol. *131*, 983–992.

Trachtenberg, S. (1998). Mollicutes —wall-less bacteria with internal cytoskeletons. J. Struct. Biol. *256*, 244–256.

Trachtenberg, S., Dorward, L.M., Speransky, V.V., Jaffe, H., Andrews, S.B., and Leapman, R.D. (2008). Structure of the cytoskeleton of Spiroplasma melliferum BC3 and its interactions with the cell membrane. J. Mol. Biol. *378*, 776–787. https://doi.org/10.1016/j.jmb.2008.02.020.

Trachtenberg, S., and Gilad, R. (2001). A bacterial linear motor: cellular and molecular organization of the contractile cytoskeleton of the helical bacterium Spiroplasma melliferum BC3. Mol. Microbiol. *41*, 827–848. https://doi.org/10.1046/j.1365-2958.2001.02527.x.

Tyanova, S., Temu, T., Sinitcyn, P., Carlson, A., Hein, M.Y., Geiger, T., Mann, M., and Cox, J. (2016). The Perseus computational platform for comprehensive analysis of (prote)omics data. Nat. Methods *13*, 731–740. https://doi.org/10.1038/nmeth.3901.

Ursell, T.S., Nguyen, J., Monds, R.D., Colavin, A., Billings, G., Ouzounov, N., Gitai, Z., Shaevitz, J.W., and Huang, K.C. (2014). Rod-like bacterial shape is maintained by feedback between cell curvature and cytoskeletal localization. Proc. Natl. Acad. Sci. U S A *111*, E1025–E1034. https://doi.org/10.1073/pnas.1317174111.

van den Ent, F., Amos, L.A., and Löwe, J. (2001). Prokaryotic origin of the actin cytoskeleton. Nature *413*, 39–44. https://doi.org/10.1038/35092500.

van den Ent, F., Izoré, T., Bharat, T.A., Johnson, C.M., and Löwe, J. (2014). Bacterial actin MreB forms antiparallel double filaments. eLife *3*, e02634. https://doi.org/10.7554/eLife.02634.

van den Ent, F., Johnson, C.M., Persons, L., de Boer, P., and Löwe, J. (2010). Bacterial actin MreB assembles in complex with cell shape protein RodZ. EMBO J. *29*, 1081–1090. https://doi.org/10.1038/emboj.2010.9.

van Teeffelen, S., Wang, S., Furchtgott, L., Huang, K.C., Wingreen, N.S., Shaevitz, J.W., and Gitai, Z. (2011). The bacterial actin MreB rotates, and rotation depends on cell-wall assembly. Proc. Natl. Acad. Sci. U S A *108*, 15822–15827. https://doi.org/10.1073/pnas.1108999108.

Vats, P., and Rothfield, L. (2007). Duplication and segregation of the actin (MreB) cytoskeleton during the prokaryotic cell cycle. Proc. Natl. Acad. Sci. USA *104*, 17795–17800. https://doi.org/10.1073/pnas.0708739104.

Wagstaff, J., and Löwe, J. (2018). Prokaryotic cytoskeletons: protein filaments organizing small cells. Nat. Rev. Microbiol. *16*, 187–201. https://doi.org/10.1038/nrmicro.2017.153.

Wang, S., Arellano-Santoyo, H., Combs, P.A., and Shaevitz, J.W. (2010). Actin-like cytoskeleton filaments contribute to cell mechanics in bacteria. Proc. Natl. Acad. Sci. U S A *107*, 9182LP–9185. https://doi.org/10.1073/pnas.0911517107.

Williamson, D.L. (1974). Unusual fibrils from the spirochete-like sex ratio organism. J.Bacteriol. *117*, 904–906. https://doi.org/10.1128/JB.117.2.904-906.1974.

Wu, L.J., and Errington, J. (1998). Use of asymmetric cell division and spoIIIE mutants to probe chromosome orientation and organization in Bacillus subtilis. Mol.Microbiol. *27*, 777–786. https://doi.org/10.1046/j.1365-2958.1998.00724.x.

Young, K.D. (2006). The selective value of bacterial shape. Microbiol.Mol. Biol. Rev. *70*, 660 LP–703. https://doi.org/10.1128/MMBR.00001-06.

STAR★METHODS

KEY RESOURCES TABLE

REAGENT or RESOURCE	SOURCE	IDENTIFIER
Antibodies		
Polyclonal rat anti-*Bacillus subtilis* MreB antibody	Rut Carballido-López	N/A
Anti-rat antibody coupled with Alexa Fluor 488	Abcam	Cat# ab150157
Bacterial and virus strains		
Spiroplasma poulsonii Ug-1	Bruno Lemaitre	N/A
Spiroplasma citri GIIX	UMR1332 "Biologie du Fruit et Pathologie," INRAE Bordeaux	N/A
Spiroplasma melliferum KC3	UMR1332 "Biologie du Fruit et Pathologie," INRAE Bordeaux	N/A
E. coli XL10 Gold	Agilent	Cat# 200,314
E. coli BL21	New England Biolabs	Cat# C2530H
E. coli MG1655 ΔmreB	Kerwyn Casey Huang	N/A
Critical commercial assays		
BACTH 2-hybrid kit	Euromedex	EUK001
Oligonucleotides		
Available in Table S2		N/A
Recombinant DNA		
Available in Table S1		N/A
Software and algorithms		
BacStalk	https://drescherlab.org/data/bacstalk/	N/A
Other		
Spiroplasma poulsonii refence genome	GenBank	JTLV02000000

RESOURCE AVAILABILITY

Lead contact

Further information and requests for resources and reagents should be directed to and will be fulfilled by the lead contact, Dr. Alexandre Persat (alexandre.persat@epfl.ch).

Materials availability

Plasmids generated in this study are available from the lead contact upon request.

Data and code availability

- Data reported in this paper will be shared by the lead contact upon request.
- This paper does not report original code
- Any additional information required to reanalyze the data reported in this paper is available from the lead contact upon request.

EXPERIMENTAL MODEL AND SUBJECT DETAILS

Bacterial strains used in this work are listed in the Key resources table. *S. poulsonii* was grown in BSK-H-spiro medium at 25°C with 5% CO2 and 10% O2 (Masson et al., 2018). Other *Spiroplasma* species were grown at ambient atmosphere at 32°C in SP4 medium. *E. coli* was grown in LB medium at 22-23°C with appropriate antibiotics when required.

METHODS DETAILS

Genetic constructs

As *Spiroplasma* have an alternative genetic code, coding sequences for MreB isoforms were codon-optimized and fully synthesized by Genewiz (South Plainfield, NJ, USA). Two constructs for each isoform, each with a different codon optimization, were ordered and indifferently used in constructs after controlling that codon optimization was not affecting the polymerization patterns. Plasmid construction (Table S1) was made by or by restriction/ligation or by Gibson Assembly, using primers listed in Table S2. Constructs were built in competent XL10-Gold cells (Agilent) and subsequently transformed in the appropriate strain for experiments.

Sequence analysis and alignment

MreB coding sequences were retrieved from the *S. poulsonii* reference genome (Accession number Genbank: JTLV02000000) and aligned using Geneious 11.0.5 (https://www.geneious.com). Similarity was calculated on the translated nucleotide sequences based on a BLOSUM45 scoring matrix. Functional sites were predicted based on previously published sequence analyses on MreBs from other *Spiroplasma* species (Takahashi et al., 2020).

Live fluorescence microcopy

E. coli was grown in LB with 50 μg/mL kanamycin for 16 to 18 hours at room temperature (22-23°C) under 300 rpm shaking. Induction was made using 100 μM IPTG for SpMreB constructs and 50 μM IPTG for EcMreB constructs, unless otherwise stated. *S. poulsonii* was extracted from *Drosophila* flies and grown in BSK-H-spiro medium at 25°C with 5%CO2 and 10% O2 (Masson et al., 2018). Bacteria were observed on glass-bottom dished with a thin agarose pad on top. Images were acquired on a Nikon Eclipse Ti-E microscope. Constructs with three different fluorescent tags were observed on a Nikon Eclipse Ti2 microscope coupled with a Yokogawa CSU W2 confocal spinning disk unit. Mechanical pressure to break cells consisted in pressing the agarose pad with the finger.

Immunofluorescence microcopy

Bacteria were grown in LB with 50 μg/mL kanamycin and 100 μM IPTG for 16 to 18 hours at room temperature (22-23°C) under 300 rpm shaking. Cells were fixed in growth medium with 1.6% formaldehyde and 0.01% glutaraldehyde for 1 h at room temperature, and immunostained as previously described (Vats and Rothfield, 2007). EcMreB was detected using a polyclonal rat anti-*Bacillus subtilis* MreB (1:300) (Jones et al., 2001) that cross-reacts with that of *E. coli* but not *S. poulsonii*, and a secondary anti-rat antibody coupled with Alexa Fluor 488 (1:1000). Cells were observed on a Nikon Eclipse Ti-E microscope using 480 nm excitation and 535 nm emission filter sets.

Western Blot

Wild-type *E. coli* MG1655 were grown in LB for 16 to 18 hours at room temperature (22-23°C) under 300 rpm shaking. *Spiroplasma citri* and *Spiroplasma melliferum* were grown for 24 hours at 29°C without shaking in SP4 medium. Cells were washed three times in PBS before being resuspended in SDS-Tris-Glycine buffer and boiled at 95°C for 15 minutes. Total proteins were then separated by SDS-PAGE, transferred to a nitrocellulose membrane and blocked for 30 minutes with 2% BSA in PBS-Tween 0.1%. MreB was detected using a polyclonal rat anti-*Bacillus subtilis* MreB (1:3000) (Jones et al., 2001) incubated overnight at 4°C and a secondary anti-rat antibody coupled with horseradish peroxydase (1:10000). Detection was performed with an ECL kit (Amersham). For normalization, an identical amount of proteins has been deposited on another SDS-PAGE run in parallel and stained with the Coomassie blue InstantBlue protein staining (Expedeon). The bioluminescence signal (MreB) was quantified using ImageJ built-in functions and normalized to the total protein amount approximated by the total InstantBlue signal.

Growth curves

A Δ*mreB* strain with pRMmreBind-2 (Shi et al., 2017), a plasmid carrying a native copy of *mreB* under control of a pLac promoter, was transformed with a pTet-SpMreB1 carrying *SpMreB1* untagged under control of a pTet promoter. pRMmreBind-2 is induced by IPTG and repressed by glucose, while pTet-SpMreB1 is induced by anhydrotetracycline (ATc). Precultures from fresh colonies were grown LB with 100 μg/mL ampicillin and 50 μg/mL kanamycin for 8 hours at room temperature (22-23°C) under 300 rpm shaking, then diluted 1:10000 in growth medium with appropriate antibiotics and induced in 96 well-plates in triplicates.

Plates were incubated under shaking at 25°C in a Tecan Infinite Pro 200 plate reader. OD_{600} was measured every 10 minutes for 20 hours.

Morphology measurements

Cell length and width were obtained from the brightfield channel of pictures acquired for filament quantification. Measurements were made using BacStalk software (Hartmann et al., 2020) with a segmentation cell size of 15 pixels, a minimum threshold of 7 pixels, and other parameters on their default value. Segmented images were manually examined to eliminate the segmentation of non-cell particles and bacteria that inactivated the transcript (no fluorescence of the GFP channel).

Bacterial two-hybrid assay

Two-hybrid assay was performed using the Bacterial Adenylate Cyclase-Based Two-Hybrid (BACTH) system (Euromedex) following the manufacturer's instructions. Each *mreB* isoform was cloned into each BACTH plasmids using standard molecular biology methods. The constructs were cotransformed two by two in chemically competent *E. coli* BTH101. 5 µL of each transformation reaction was spotted on LB plates with 50 µg/mL kanamycin, 100 µg/mL ampicillin, 500µM IPTG and 40 µg/mL X-gal. Plates were incubated at 30°C for 48h prior to photography on a lightbox.

Sample preparation for co-immunoprecipitation

Bacterial cultures were performed as for microscopy experiments. 2 mL of overnight *E. coli* culture expressing single isoform with a GFP tag (or GFP alone as a negative control) were harvested, resuspended in 500 µL of Glucose-Tris-EDTA buffer (50mM glucose, 10 mM EDTA, 25 mM Tris-HCl pH 8) with 50 µg/mL of lysozyme and incubated 20 minutes at room temperature. DNAse I (1 µg/mL) and NP40 0.05% were then added to tubes, and samples were homogenized with 100 µm diameter glass beads on a Precellys Evolution (Bertin Technologies). Debris were pelleted for 1 minute at 10000 g and the supernatant was used for the first incubation.

S. poulsonii was cultured as previously described (Masson et al., 2018)(Masson et al., 2018). 80 mL of 1 week-old culture was pelleted by 20 minutes centrifugation at 10000 g at 18°C, washed twice with PBS 1.5X, and resuspended in 3 mL of lysis buffer (Tris 50 mM pH7.2, NaCL 300 mM, PMSF 1 mM, DNAse I 1 µg/mL, NP40 0,05%). Cells were homogenized with 100 µm diameter glass beads on a Precellys Evolution (Bertin Technologies) and incubated 20 minutes at room temperature, then for 2h on ice. Debris were pelleted for 1 minute at 10000 g and the supernatant was used for the second incubation.

Co-immunoprecipitation

20 µL of GFP-Trap Magnetic Beads (Chromotek) were used for each sample, following the manufacturer's instruction for preparation and magnet-washes. Beads were washed with 180 µL of PBS-Tween 20 (PBS-T) 0.1%, then saturated for 20 minutes with 2% BSA in PBS-T. 300 µL *E. coli* samples were then incubated for 1h at room temperature on a spinning wheel, and washed three times with PBS-T. 300 µL of *S. poulsonii* samples were then incubated on the beads for 1h30 at room temperature on a spinning wheel, and washed twice with PBS-T and once with mQ water. Elution was made by boiling the beads in 50 µL of Tris-Glycine SDS Running Buffer (Novex) for 5 min at 95°C. Each sample was made in triplicate. The protein concentration was assessed using the Pierce BCA Protein Assay Kit (Thermo Fisher Scientific) and 20 µg of sample was mixed with NuPage LDS buffer 1X final (Invitrogen) and 20 µM DTT.

LC-MS/MS and data analysis

LC-MS/MS and data analysis was performed at the Proteomics Core Facility of EPFL. Samples were separated by SDS-PAGE on a 10% polyacrylamide gel and stained with Coomassie blue. Each gel lane was entirely sliced and proteins were In-gel digested (Dorin-Semblat et al., 2015). Resulting peptides were desalted on StageTips(Rappsilber et al., 2007) and dried under a vacuum concentrator. For LC-MS/MS analysis, resuspended peptides were separated by reversed phase chromatography on a Dionex Ultimate 3000 RSLC nano-UPLC system in-line connected to an Orbitrap Lumos Tribrid mass spectrometer (Thermo Fisher Scientific, Waltham, USA). Raw data were processed using MaxQuant 1.6.10.43 (Cox and Mann, 2008) against a concatenated database consisting of the Uniprot *Spiroplasma poulsonii* protein database (2003entries LM201017), the Uniprot *Escherichia coli* protein database (4391 entries LM201019) and a list of $MreB^{GFP}$ sequences used as baits. In order to reduce observed protein grouping artefacts resulting from

the insertion of an internal GFP stretch into bait sequence constructs, the GFP stretch was manually removed. Carbamidomethylation was set as fixed modification, whereas oxidation (M), phosphorylation (S, T, Y), acetylation (Protein N-term) and glutamine to pyroglutamate were considered as variable modifications. A maximum of two missed cleavages were allowed and "Match between runs" option was enabled. A minimum of 2 peptides was required for protein identification and the false discovery rate (FDR) cutoff was set to 0.01 for both peptides and proteins. Label-free quantification and normalisation was performed by Maxquant using the MaxLFQ algorithm, with the standard settings (Cox et al., 2014).

QUANTIFICATION AND STATISTICAL ANALYSIS

Softwares

The data were analyzed using R version 4.1.1 and Prism version 8.4.3.

Quantitative filament analysis

The extremely high diversity of patterns that we uncovered with tagged SpMreB made already published segmentation methods inefficient, as well as machine-learning based image analysis. Images were thus manually screened and bacteria were classified according to the major pattern observed. Bacteria with no clear pattern were classified as "others" and not accounted for in the figures (<1% of observations). Bacteria were randomly picked from at least two fields of view per replicate, and three independent replicates per construct, until reaching a minimum of 300 observations per construct.

Morphology measurements

Length and width data were acquired from at least 50 cells on 5 or 6 different fields of view using BacStalk. Data were analyzed by ANOVA followed by Tukey HSD post-hoc testing.

Co-immunoprecipitation data analysis

The data were processed using Perseus version 1.6.12.0(Tyanova et al., 2016) from the MaxQuant tool suite. Reverse proteins, potential contaminants and proteins only identified by sites were filtered out as well as the protein groups from *E. coli* proteome. Protein groups containing at least two valid values in at least one group were conserved for the following analysis. Empty values were imputed with random numbers from a normal distribution (Width: 0.5 and down shift: 1.9 sd). A two-sample t-test with permutation-based FDR statistics (250 permutations, FDR = 0.05, S0 = 0.5) allowed determining significant candidates.